www.pss-a.com

ZnO Thin Films Grown by Plasma-Enhanced Atomic Layer Deposition: Material Properties Within and Outside the "Atomic Layer Deposition Window"

Julian Pilz, Alberto Perrotta, Günther Leising, and Anna Maria Coclite*

ZnO thin films and nanostructures are applied in various devices due to their interesting optical and electrical properties. Atomic layer deposition (ALD) of ZnO offers unique advantages such as precise thickness control, uniformity, and conformality. Using reactive plasma species as the co-reactant (PE-ALD) allows further enhancement of the material characteristics and tunable properties. The substrate temperature has been reported to be the most influential parameter in this technique, as it affects the growth per cycle (GPC) and material properties. However, an investigation on how the film properties are linked to the GPC is lacking in the literature. Herein, the temperature dependence of several material properties is found closely related to the GPC. The preferential crystal orientation switches from (100) to (002) up to the constant region of the GPC versus temperature, the so-called ALD window. Refractive index and mass density show different slopes in temperature regions outside and within the ALD window. Excitonic absorption is only found for films prepared within the ALD window, and the resistivity drops rapidly above the ALD window. Following these results, more insights can be gained on the ALD growth (especially the role of the ALD window) and ideal temperature ranges for specific applications.

1. Introduction

ZnO attracts great attention due to its direct wide bandgap and interesting optical, electrical, and piezoelectric properties.[1] In its thin film or nanostructure form, these properties have been exploited for applications such as transparent conductive oxides,[2,3] resistance random access memories,[4,5] gas sensors,[6,7] and piezoelectric generators.[8,9]

Among the techniques used to deposit ZnO thin films, atomic layer deposition (ALD) stands out due to the possibility to

J. Pilz, Dr. A. Perrotta, Prof. G. Leising, Prof. A. M. Coclite
Institute of Solid State Physics
NAWI Graz
Graz University of Technology
8010 Graz, Austria
E-mail: anna.coclite@tugraz.at

The ORCID identification number(s) for the author(s) of this article can be found under https://doi.org/10.1002/pssa.201900256.

conformally coat complex structures, precise thickness control (in the Å-range), and relatively low deposition temperatures.[10,11] One cycle in the ALD process comprises the sequential exposure of the substrate to two (or more) precursors, separated by purge steps. This cycle is repeated until the desired thickness is achieved. As the surface reactions during the respective steps in a cycle are self-limiting, the growth per cycle (GPC) is typically less than a monolayer and in the Å cycle^{-1} range.

Most investigations on ALD of ZnO adopt diethylzinc (DEZ) and water as the precursor and co-reactant, respectively. The surface reactions in this case are driven by thermal energy, and the substrate is heated during the deposition. This process is usually referred to as thermal ALD. A variant is plasma-enhanced atomic layer deposition (PE-ALD), in which reactive plasma species are utilized as co-reactants instead of water.[12] The advantages of using PE-ALD instead of thermal ALD include often a higher growth rate, improved material characteristics at lower substrate temperature, and the possibility to tune material properties by changing the plasma characteristics.[12–14]

The substrate temperature has been reported to be the most influential deposition parameter in both thermal ALD and PE-ALD.[11] The GPC shows a strong temperature dependence outside the so-called ALD window, a region in which it stays constant. (This in our opinion is the most commonly used (though controversial) definition of the term ALD window in the literature. Other definitions have been used[15] referring to a temperature range in which the criterion of self-terminating reactions is fulfilled without the necessity of having a constant GPC versus temperature.) Within the ALD window, the growth mechanism is considered to happen in an ideal ALD manner, i.e., complete and self-limiting surface reactions.[10] Furthermore, the substrate temperature strongly affects the structure, stoichiometry, and amount of defects of the ZnO films and, in turn, device-related optical and electrical properties. While the temperature dependence of the GPC for PE-ALD of ZnO has been investigated by several groups over a wide temperature range,[13,16–20] material or device properties have often been described independently of the growth behavior. The crystallinity and texture of PE-ALD ZnO films have been shown to be strongly affected by the substrate temperature. A switch from (100)

preferential orientation at lower temperature to (002) for higher temperatures has been shown by Park et al.,[16] Zhang et al.,[20] and Rowlette et al.[17] Likewise, a switch from no preferential orientation to (002) preferential orientation was shown by Kim et al.[13] In all these cases, the temperature at which this switch happens seems to be closely related to the beginning of the reported ALD window. A discussion on how a switch in the preferential orientation affects the GPC is missing in these publications. Photoluminescence (PL) was also shown to depend on the substrate temperature and is an indicator for the optical quality and defects in the ZnO films. While the PL spectra showed a significant near-band-edge emission (i.e., high optical quality) for samples prepared within the ALD window,[13,17,20] defect-related emission bands were observed for substrate temperatures below[17,20] or above[13] the ALD window. Kim et al.[13] furthermore showed that the resistivity decreased drastically for ZnO films prepared at temperatures above the ALD window, correlating it with an increase in the defect carrier concentration. The temperatures, at which these changes in material properties occur, differ among the publications. However, when analyzing the temperature trend of the material properties and the GPC within a publication, the trends often seem to correlate.

The aim of the present publication is therefore to link the temperature dependency of several material properties to the temperature behavior of the GPC, especially focusing on regions below, within, and above the ALD window. By this, a more detailed description of the ALD growth regimes of ZnO is presented, as well as general directions to select the right temperature region for specific applications.

2. Results and Discussion

The dependence of the GPC with respect to the substrate temperature is shown in **Figure 1**a. It was found to rapidly increase with the substrate temperature, from 1.6 Å cycle^{-1} at 25 °C to around 2.5 Å cycle^{-1} at 125 °C. In the range of 125 to 200 °C, the GPC was constant and therefore we identified this region as the so-called ALD window.[10] The thickness deposited per cycle in the ALD window with a value around 2.5 Å is comparable with the interplanar spacing along the *c*-axis of the ZnO wurtzite crystal structure (2.60 Å). The crystalline properties and texture of the films are discussed in detail later, showing the correlation between the ALD window and the structural parameters. Further increase in the substrate temperature leads to a rapid increase in the GPC. In addition, the standard deviation in this region significantly increases, pointing out a spatial dependence of the growth in the reactor, typical of a chemical vapor deposition (CVD) component in the growth. Different effects have been proposed to explain the temperature dependency of the GPC. At temperatures below the ALD window, not enough energy is delivered to the system to complete all surface reactions leading to lower GPC.[21] At temperatures above the ALD window, precursor molecules instead decompose into smaller fragments, leading to an accelerated CVD-like growth and an increase in GPC.[13,19,21] At the same time, desorption of precursor molecules can take place, leading to a decrease in GPC at high temperatures.[20,21] In addition, as ALD growth happens ideally in a monolayer-by-monolayer fashion, the GPC will also be
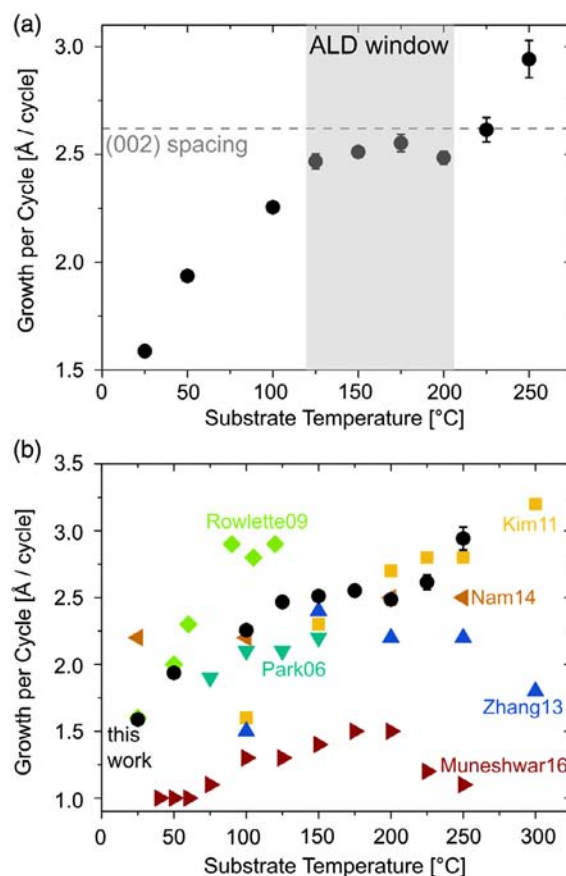

Figure 1. a) Growth per cycle with respect to the substrate temperature of samples prepared on Si substrates. The gray area marks the ALD window, in which the GPC stays constant. The error bars are plotted for each data point but are within marker size in most cases. The size of the unit cell along the c-axis of the ZnO wurtzite crystal structure is indicated by the dashed line. b) Comparison of the results from (a) with selected literature results. An error of ±0.1 Å cycle^{-1} has to be taken in to account for the literature results. References are given in the main text.

influenced by the lattice spacing when growing crystalline films. As the preferential orientation and thus the lattice spacing normal to the substrate can change with temperature,[22] so will the GPC. These different effects happen simultaneously, making their individual effects on the GPC difficult to distinguish. On the other hand, especially for PE-ALD, self-limiting growth can be achieved well below the ALD window.[14,23] This raises questions about the definition and relevance of the ALD window (in PE-ALD processes) and the often exclusive focus on properties at temperatures within the window. For this reason, an analysis of the opto-chemical and structural properties of ZnO layers as a function of the relative position of their deposition temperature with respect to the ALD window will help in correlating process parameters and material properties in a more rigorous way.

In the literature, a similar behavior of the GPC with respect to substrate temperature has been reported, i.e., a steep increase toward a constant regime with increasing temperature, and either an increase or decrease for temperatures higher than the ALD window. A selection of literature results[13,16–20] on

PE-ALD ZnO for the temperature behavior of the GPC in comparison with this work is shown in Figure 1b.

While the general trend of the data in the figure is similar, the obtained values of the various publications differ largely. This difference is especially highlighted in the start, end, and width of the ALD window as well as the values of the GPC, and it was suggested to mostly stem from differences in the reactor designs.[11] Nevertheless, an ALD window has been observed in all the aforementioned publications.

The crystalline properties investigated by specular X-ray diffraction (XRD) are shown in **Figure 2**. At room temperature, the ZnO films exhibit a polycrystalline pattern with a (100) texture, as reported in a previous publication.[14] By increasing the substrate temperature, the contribution of (002) peak increases and becomes the dominant orientation. In detail, for temperatures higher than 100 °C, the crystallites are highly oriented in the [002] direction and the (100) peak is drastically reduced in intensity. A (100) or (002) texture can thus be obtained by applying either a low or high substrate temperature, respectively. A similar behavior was observed by Zhang et al.,[20] but temperatures below 100 °C were not investigated in their study. Depositing crystalline films with a texture at temperatures below 100 °C could, however, be beneficial for applying functional ZnO films on thermo-sensitive substrates (e.g., polymers[25–27] or biomaterials[28,29]). On the other hand, a (002) texture is often desired in piezoelectric[8,30] or optoelectronic[31,32] applications, as the c-axis (i.e., the polar axis) of the ZnO crystallites is oriented perpendicular to the substrate plane.

By comparing the crystalline properties with respect to the ALD window, the following observations can be made. Below the ALD window (25–100 °C), we can observe both the (100) and the (002) peak. There is a mixture of both orientations, whereas the (002) orientation becomes the dominant one at higher temperatures. Inside the ALD window (125–200 °C), the films are highly (002) textured and show enhanced crystallinity. As mentioned earlier, the GPC within the ALD window ($\approx$2.5 Å cycle^{-1}) is close to the interplanar spacing of the (002)

orientation (2.60 Å). The interplanar spacing of the ZnO wurtzite structure oriented along the (002) and the (100) planes is sketched in **Figure 3**. Looking at the atomic arrangement of both orientations, the (002) planes parallel to the substrate consist of atoms of only one species, whereas the planes of the (100) orientation consist of alternating Zn and O atoms. This would suggest that not a full crystalline plane with (100) orientation can be grown within one cycle in the ALD process, but the GPC is restricted to half of the lattice spacing (2.82 Å / 2 = 1.41 Å). Thus, the crystal orientation at temperatures below the ALD window together with the not complete surface reactions could explain the lower GPC that we observe at those temperatures. For temperatures above the ALD window, the GPC increases to values larger than the (002) interplanar spacing, whereas the XRD results show a strong preferential (002) orientation. Thus, in this temperature region, the growth cannot happen in a monolayer-by-monolayer fashion anymore but includes a CVD-component in the mechanism. This component also accounts for the large standard deviation of GPC values at these temperatures, reported in Figure 1a.

The relationship between texture and GPC in thermal ALD of ZnO (applying DEZ and water) has been investigated by Yousfi et al.[33] They found a (100) preferential orientation within the ALD window and a GPC in between 1 and 2 monolayers of the (100) orientation. The GPC values larger than a monolayer were attributed to the possible presence of roughness. In other publications on thermal ALD,[34–37] a transition from (002) to (100) preferential orientation with temperature was reported, often accompanied with a drop in (002) peak intensity at the edges of the ALD window. Within the ALD window, both (100) and (002) orientations were apparent with no strong preferential orientation and a GPC of around 2 Å. These GPC values lie in between the (100) spacing (1.41 Å) and the (002) spacing (2.60 Å). This is an indicator that the GPC within the ALD
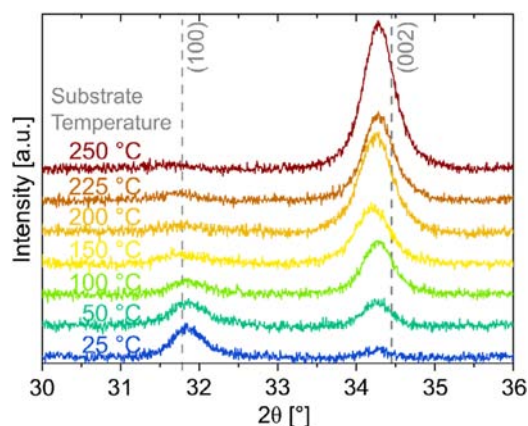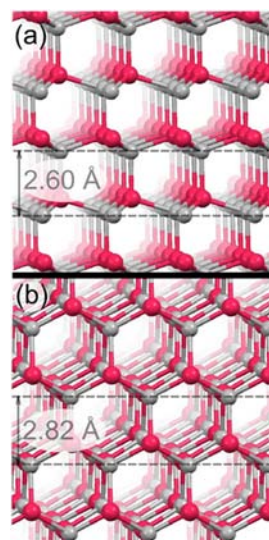

Figure 2. Specular XRD spectra of samples prepared on glass substrates at different substrate temperatures. The spectra are stacked for clarity. Vertical, dashed lines show the peak positions of a ZnO powder reference (ICSD-26170).[24] A shift to smaller angle (i.e., larger lattice spacing) compared with the powder pattern is apparent for the (002) peak, which may originate from microstrain in the sample.

Figure 3. Sketch of the atomic configuration of the ZnO wurtzite crystal structure with a) (002) orientation and b) (100) orientation. Gray and pink atoms correspond to Zn and O, respectively. The sketch was obtained using the Mercury 3.10.3 software and with the lattice parameters of ICSD-26170.[24]

window is strongly correlated to the preferential orientation also for thermal ALD. At high temperatures above the ALD window, the preferential orientation switched back to (002).[33,35]

The refractive index and the mass density of the films are shown in **Figure 4**. The refractive index values were obtained by applying a Cauchy model to the SE data and are reported for a wavelength in the ZnO transparent region (633 nm). The mass density was obtained by measuring the critical angle α_c by XRR and applying the following formulas.[38] The electron density can be calculated as

$$\rho_e = \left(\frac{\alpha_c}{\lambda}\right)^2 \times \frac{\pi}{r_e} \tag{1}$$

where ρ_e is the electron density, α_c is the critical angle from the XRR measurement, $\lambda = 1.5418$ Å wavelength of the Cu Kα radiation, $r_e = 2.818 \times 10^{-15}$ m is the classical electron radius.

The mass density can then be derived from

$$\rho = \frac{\rho_e}{N_{e,ZnO}} \times \frac{M_{ZnO}}{N_A} \tag{2}$$

where ρ is the mass density, ρ_e is the electron density from (1), $N_{e,ZnO} = 38$ is the number of electrons in the ZnO molecule, $M_{ZnO} = 81.38$ g mol^{-1} is the molar mass of ZnO, $N_A = 6.022 \times 10^{23}$ mol^{-1} is the Avogadro constant.

Both the refractive index and the mass density show trends in regions corresponding to the ALD window. The refractive index shows a strong rapid increase from 1.90 at room temperature up to 1.93 at the start of the ALD window. In this region, the XRD results pointed out a switch from (100) to (002) texture. In the ALD window, the increase slows down, and XRD results showed a more pronounced (002) peak with increasing temperature. Above the ALD window, a rapid drop down to 1.86 can be observed for the refractive index. Similarly, the mass density slightly increases below the ALD window, strongly increases within the ALD window, and decreases again above the ALD window. Please note that for calculating the mass density, ideal ZnO bulk values are assumed. Nonstoichiometric films could therefore lead to values that are above the literature value for
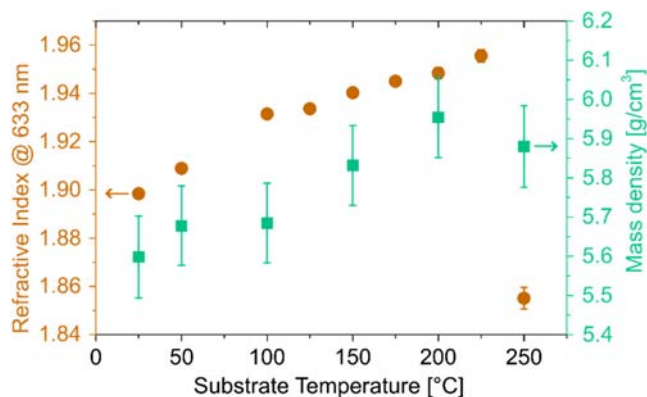
ZnO[39] ($\rho = 5.61$ g cm^{-3}). In fact, X-ray photoelectron spectroscopy (XPS) analysis points out an increase in Zn/O ratio for higher temperatures (Figure S1, Supporting Information), which has also been reported for thermal ALD of ZnO.[40] However, the trend for the mass density is valid as the measured electron density is only multiplied by a constant to obtain the mass density.

Transmission spectra obtained by UV–vis spectroscopy are shown in **Figure 5**a. All the films are highly transparent (transmission >90%) over most of the visible light range, sufficient for its use as a transparent electrode (when doped, e.g., with Al)[41] or as a buffer layer[42] in photovoltaic devices. At around 500 nm, the films start to absorb and the transmission decreases rapidly. Interesting features can be observed around the bandgap that can be better followed in Figure 5b, in which the absorption coefficient is plotted over energy in the region marked in Figure 5a. The absorption coefficient was calculated from the transmission values by $\alpha = -\frac{\log(T)}{d}$, with α being the absorption coefficient, T the transmission, and d the layer thickness. Below the band edge, α includes contributions from reflection; it is however well represented above the band edge.

For films deposited at temperatures below the ALD window (25 and 50 °C) the absorption coefficient shows a rather smooth transition from transmitting to the absorbing region, while it becomes sharper with temperatures within the ALD window.
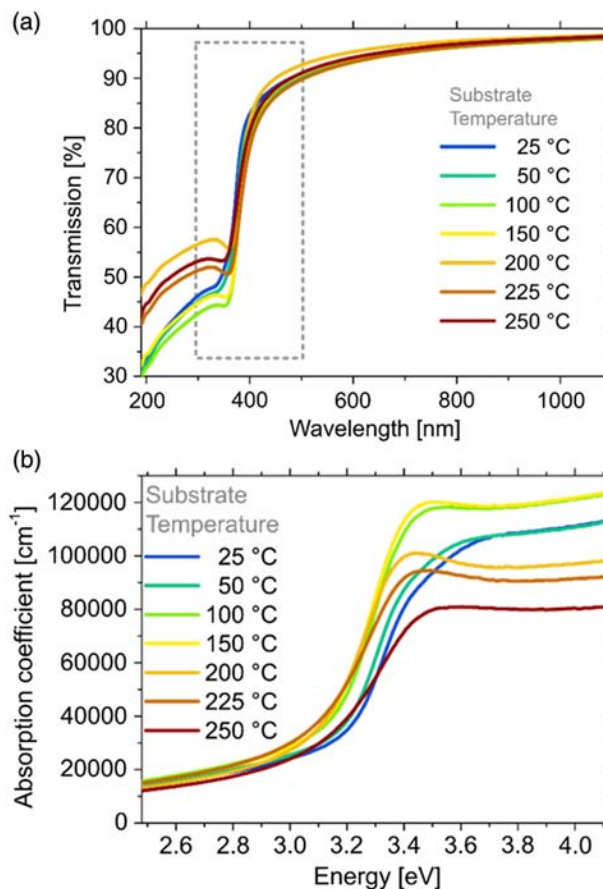

Figure 4. a) Refractive index at 633 nm obtained from SE (circles) and b) mass density obtained from XRR (squares) as a function of substrate temperature for samples prepared on Si substrates. Error bars are plotted for all data points but are only visible for some.

Figure 5. a) UV–vis transmission spectra of samples prepared at different substrate temperatures on quartz substrates and b) absorption coefficient from the region around the band edge region highlighted in (a).

At 250 °C (above the ALD window), the transition becomes again very smooth. A sharper transition in the absorption spectra can be attributed to a higher optical quality within the ALD window, i.e., less amount of defect absorption states.[43] Furthermore, for samples prepared within the ALD window, a peak at around 3.4 eV was observed. The peak can be attributed to the formation of excitons. Observing these excitonic features at room temperature (for films deposited within the ALD window) points out a high structural quality of these thin films.[44,45] This property, combined with the significantly lower substrate temperature compared with other techniques (such as pulsed laser deposition[44]) and the possibility to conformally coat complex structures, makes PE-ALD an attractive deposition technique for functional optical devices.[46] As an example, UV lasing has been reported for ZnO thin films, which is based on stimulated excitonic emission.[1,32,47]

The absorption edge could be obtained via Tauc-fitting from the absorption coefficient spectra. As ZnO has a direct bandgap, the absorption coefficient reads

$$\alpha(E) = \frac{A}{E}(E - E_g)^{\frac{1}{2}} \quad (3)$$

with A a constant and E_g the bandgap. Thus, by plotting $(\alpha E)^2$ over E, the bandgap can be extracted by extrapolating the linear region to 0 (Tauc plot; example shown in Figure S2, Supporting Information).[43,48] It was, however, reported that this fitting procedure does not give the real bandgap value in the presence of an excitonic peak in the absorption spectrum but rather the onset of the absorption edge.[48] The absorption edge obtained from both SE and UV–vis measurements is plotted in **Figure 6**.

The absorption edge obtained from UV–vis measurements shifts to lower energy (red shift) with increasing temperature from 3.22 eV at room temperature to 3.15 eV at 225 °C. A red shift of the absorption edge with increasing substrate temperature has been observed in thermal ALD[49] and CVD[50] of ZnO. In the thermal ALD reference,[49] Yuan et al. found a reverse relationship between the refractive index and the bandgap with increasing substrate temperature, which is in line with our results (Figure 4). Furthermore, the near-bandgap-emission (in PL) showed a red shift and high intensity (accompanied by
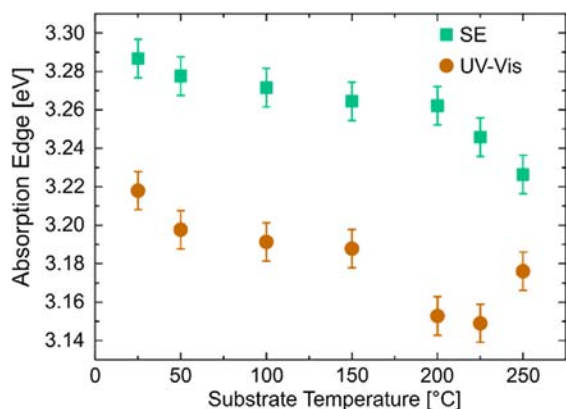
increased crystal quality) at high temperature. Tan et al.[50] performed CVD of ZnO and found a red shift of the bandgap with increased substrate temperature due to crystallization of amorphous regions. Moreover, a red shift of the absorption edge has been observed in annealing procedures of ZnO, associated with an enhanced removal of intrinsic defects and improved crystallinity at a higher annealing temperature.[51,52] The absorption edge increases by around 30 meV when the substrate temperature is further increased from 225 to 250 °C. This phenomenon could be explained by the Burstein-Moss effect caused by an enhanced free electron density and thus filling of lower states in the conduction band.[53] This would also agree well with the resistivity drop in **Figure 7**. The absorption edge shift could thus be explained by an interplay of changes in the crystalline structure (Figure 2) and defect density. A detailed analysis of the defects by, e.g., PL is, however, not within the scope of this article. Also for the absorption edge obtained from SE measurements, a red shift can be observed. However, an offset is apparent, with the SE results being around 70 meV higher than the UV–vis results. This is attributed to the limited measurement range of the available ellipsometer (370–1000 nm), being able to measure only the foot region of the absorption. The limited measurement range leads to a different slope in the Tauc-fitting and consequently to an offset (and further decrease instead of an increase of the absorption edge at 225 to 250 °C) compared with the evaluation of the UV–vis measurements.

The resistivity of the films was obtained by four-point-probing and is shown in Figure 7. Films prepared below or within the ALD window (25–200 °C) have a high resistivity, which was too high to measure with the available setup. Above the ALD window (225–250 °C), films show a decrease in resistivity over several orders of magnitude, reaching around 10 Ωcm at 250 °C. As already mentioned, the drop in resistivity accompanied by the increase of the absorption edge could be described by the Burstein-Moss effect. Kim et al. found a similar behavior in PE-ALD ZnO;[13] in their case, the resistivity dropped over 6 orders of magnitude when increasing the substrate
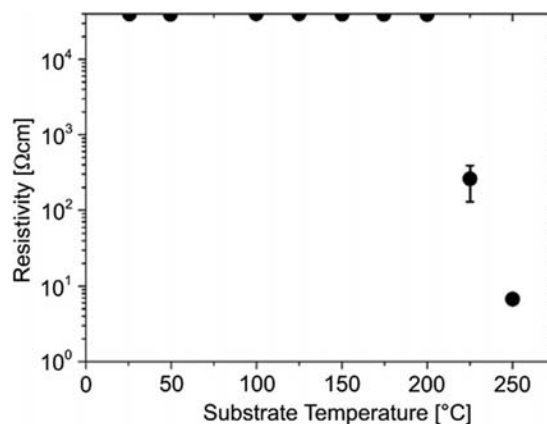

Figure 6. Absorption edge as a function of substrate temperature obtained from Tauc fitting from SE (square) and UV–vis (circle) measurements. Samples prepared on Si (SE) or quartz (UV–vis) substrates.

Figure 7. Resistivity measured by four-point-probing (inline, at room temperature) as a function of substrate temperature for sample prepared on glass substrates. Half circles on the top axis depict resistivity values that were too high to measure (>4 × 10⁴ Ωcm). Standard deviation results from measuring two samples and several measurement points around the center.

temperature from 225 to 300 °C. They showed that the decrease in resistivity was caused by an increase in carrier concentration. Further studies on thermal ALD ZnO showed that zinc interstitials can play a major role in the conduction mechanism of films deposited at a higher substrate temperature.[53,54] It is fair to assume that in our case the drop in resistivity above the ALD window is caused by zinc-related defects. The drop in refractive index, the loss of excitonic absorption, and the slightly nonstoichiometric composition point in the same direction.

Regarding possible applications, films within the ALD window have high resistivity and strong (002) preferential orientation, both prerequisites for piezoelectrics.[55] On the other hand, films prepared (slightly) above the ALD window showed lower resistivity and high transmission, pointing out a possible application (with Al doping) for transparent conductive oxides.[2]

3. Conclusion

In this contribution, the temperature-dependent growth of ZnO thin films, deposited by PE-ALD, was investigated. The growth per cycle was constant at $\approx 2.5\,\text{Å cycle}^{-1}$ in the range of 125–200 °C, which was identified as the ALD window. The GPC within the ALD window was shown to be just below the lattice spacing of the (002) orientation (2.60 Å) pointing out a growth close to a monolayer-by-monolayer growth. Above the ALD window, the GPC started to increase rapidly with increased standard deviation, pointing out a possible CVD-component in the growth.

Structural and optical material properties were investigated, which showed a different behavior in regions closely related to the temperature regions defined by the GPC (below, within, and above the ALD window).

The specular orientation measured by XRD showed a (100) preferential orientation at 25 °C. The (002) peak increased with increasing temperature and became the preferential orientation within the ALD window and above.

The refractive index (at 633 nm) measured by SE exhibited a strong increase from 1.90 to 1.93 below the ALD window (25–100 °C). The increase slowed down for temperatures within the ALD window and slightly above (125–225 °C), reaching a value of 1.96 at 225 °C. Above the ALD window (250 °C), the refractive index dropped rapidly to 1.86. Similarly, the mass density showed two slopes below and within the ALD window and a decrease above the ALD window.

UV–vis spectroscopy showed that all samples were highly transparent ($\approx$90% transmission) over most of the visible range. Samples prepared at temperatures within the ALD window and slightly above (100–225 °C) exhibited a peak that could be attributed to excitonic absorption. The absorption edge was found to red shift with increasing substrate temperature until 225 °C and increased again at 250 °C (possibly due to the Burstein-Moss effect).

The resistivity of the samples (measured at room temperature) was very high ($>4 \times 10^4\,\Omega\text{cm}$) for samples below and within the ALD window and dropped above the ALD window to $10\,\Omega\text{cm}$ at 250 °C.

Regarding device applications, ZnO films prepared below the ALD window could be useful for application on thermosensitive substrates in which polycrystalline films are necessary. Films

prepared within the ALD window are more textured, exhibit excitonic absorption, and have high resistivity. Typical application fields would be therefore in optical devices such as UV–lasers or piezoelectrics. Films prepared above the ALD window show a drop in resistivity and could therefore be used as a basis for transparent conductive oxides, however exhibiting less uniform growth.

4. Experimental Section

ZnO thin films were deposited using a custom-built direct plasma ALD reactor. The reactor was in an asymmetric plate configuration, and the clearance between the top showerhead radio frequency (RF) electrode and the heating stage (Yuheng Electric Heating Technology Co., Ltd) was 5 cm. DEZ (optoelectronic grade, Dockweiler Chemicals) was used as the metalorganic precursor and was pulsed into the reactor using an ALD-valve (Swagelok ALD3) without additional heating or bubbling system. An RF-power generator (Advanced Energy Cesar 13.56 MHz) combined with a matching network (Advanced Energy Navio) served as the power source for the O_2-plasma. The pumping system consisted of a turbomolecular pump (Pfeiffer vacuum TMH071P) and a rotary vane pump (Pfeiffer vacuum DUO5M). The pressure in the reactor was $\approx$75 mTorr during plasma exposure. The flow rates of O_2 and Ar were set to 20 sccm during the plasma and purging step, respectively, using a multi gas controller (MKS 647C) and mass flow controllers (MKS MF1-C).

The ALD process consisted of the repetition of the following four steps 1) DEZ dose; 2) Ar purging; 3) O_2-plasma dose (including a 10 s O_2-flow stabilization step prior to the plasma ignition); and 4) Ar purging. Prior to the deposition, the samples were exposed to 8 s O_2-plasma to activate the surface. The RF-power for the plasma dose was fixed at 60 W for all depositions. The saturation behavior of the four steps was investigated at room temperature,[14] and due to possible decomposition effects of DEZ,[19] the saturation of the purging step after DEZ was also investigated at 250 °C. At higher temperatures, the growth was found to be self-limiting when the recipe was fixed at 0.15 s for the DEZ dose, 22 s for the Ar purge, 8 s for the O_2-plasma dose, and 15 s for the second Ar purge. This recipe was applied to all temperatures investigated. The setup was controlled by an Arduino microcontroller and an in-house written *Python* program. The ZnO films were grown on single-side polished Si (100) substrates with a native oxide layer for spectroscopic ellipsometry and X-ray reflectivity, on quartz substrates (Esco Optics) for UV–vis spectroscopy, and on glass substrates for X-ray diffraction and four-point probing. The films were prepared at substrate temperatures ranging from room temperature to 250 °C. The growth per cycle (GPC) for each deposition was obtained by dividing the mean value of the film thickness of three samples, placed on different positions on the substrate heater, by the number of cycles. Due to the temperature-dependent GPC, the number of cycles for each of the respective depositions at different temperatures was modified to obtain film thicknesses in the range of 25–34 nm.

Spectroscopic ellipsometry (SE, J.A. Woollam M-2000V) was used to determine the thickness and optical constants of the films. Measurements were carried out in a wavelength range of 370–1000 nm at three different angles (65°, 70°, and 75°). Using a Cauchy model in the transparent region of the ZnO films (450–1000 nm), it was possible to extract the thickness and refractive index of the film.

UV–vis spectroscopy (Shimadzu UV-1800) was used to measure the transmission of the films in a wavelength range from 190 to 1100 nm, and the absorption edge could be extracted via Tauc fitting.[14,43] Contributions from reflections were neglected in the analysis.

XRD in a θ/θ-configuration (Panalytical Empyrean) utilizing monochromatized copper radiation ($\lambda = 1.5418\,\text{Å}$) was used to analyze the specular crystalline properties of the films. The diffractometer's PIXcel^{3D}-detector was operated in 1D-mode and a 1/8° divergence slit, a 10 mm mask, and a P7.5 antiscatter slit were used in the setup. Furthermore, X-ray reflectivity (XRR) measurements were performed to gain information on the electron density and, from that, the mass density

was derived. The measurements were performed on the same system as the XRD measurements, but adopting a 1/32° divergence slit and a P0.1 antiscatter slit. The detector was operated in point mode with three channels.

Four-point-probing (Jandel Universal Probe Station, tip spacing 1 mm inline) was performed on films deposited on 2.5×2.5 cm glass substrates at room temperature. The resistivity was calculated by

$$\rho = 4.45 \times \frac{U}{I} \times t \tag{4}$$

and U and I are the measured voltage and current, respectively, 4.45 is a geometry factor, and t is the mean layer thickness from SE measurements.

Supporting Information

Supporting Information is available from the Wiley Online Library or from the author.

Conflict of Interest

The authors declare no conflict of interest.

[1] Ü. Özgür, Y. I. Alivov, C. Liu, A. Teke, M. A. Reshchikov, S. Doğan, V. Avrutin, S.-J. Cho, H. Morkoç, *J. Appl. Phys.* **2005**, *98*, 041301.

[2] P. Banerjee, W.-J. Lee, K.-R. Bae, S. B. Lee, G. W. Rubloff, *J. Appl. Phys.* **2010**, *108*, 043504.

[3] D.-J. Lee, H.-M. Kim, J.-Y. Kwon, H. Choi, S.-H. Kim, K.-B. Kim, *Adv. Funct. Mater.* **2011**, *21*, 448.

[4] W.-Y. Chang, Y.-C. Lai, T.-B. Wu, S.-F. Wang, F. Chen, M.-J. Tsai, *Appl. Phys. Lett.* **2008**, *92*, 022110.

[5] S. Kim, H. Moon, D. Gupta, S. Yoo, Y.-K. Choi, *IEEE Trans. Electron Devices* **2009**, *56*, 696.

[6] L. Zhu, W. Zeng, *Sens. Actuators A, Phys.* **2017**, *267*, 242.

[7] Q. Wan, Q. H. Li, Y. J. Chen, T. H. Wang, X. L. He, J. P. Li, C. L. Lin, *Appl. Phys. Lett.* **2004**, *84*, 3654.

[8] Z. L. Wang, J. Song, *Science.* **2006**, *312*, 242.

[9] G. Zhu, R. Yang, S. Wang, Z. L. Wang, *Nano Lett.* **2010**, *10*, 3151.

[10] S. M. George, *Chem. Rev.* **2010**, *110*, 111.

[11] T. Tynell, M. Karppinen, *Semicond. Sci. Technol.* **2014**, *29*, 043001.

[12] H. B. Profijt, S. E. Potts, M. C. M. de Sanden, W. M. M. Kessels, *J. Vac. Sci. Technol. A Vacuum, Surfaces, Film.* **2011**, *29*, 50801.

[13] D. Kim, H. Kang, J.-M. Kim, H. Kim, *Appl. Surf. Sci.* **2011**, *257*, 3776.

[14] J. Pilz, A. Perrotta, P. Christian, M. Tazreiter, R. Resel, G. Leising, T. Griesser, A. M. Coclite, *J. Vac. Sci. Technol., A* **2018**, *36*, 01A109.

[15] R. L. Puurunen, *J. Appl. Phys.* **2005**, *97*, 121301.

[16] S.-H. K. Park, C.-S. Hwang, H.-S. Kwack, J.-H. Lee, H. Y. Chu, *Electrochem. Solid-State Lett.* **2006**, *9*, G299.

[17] P. C. Rowlette, C. G. Allen, O. B. Bromley, A. E. Dubetz, C. A. Wolden, *Chem. Vap. Depos.* **2009**, *15*, 15.

[18] T. Nam, C. Wan Lee, H. Jae Kim, H. Kim, *Appl. Surf. Sci.* **2014**, *295*, 260.

[19] T. Muneshwar, G. Shoute, D. Barlage, K. Cadien, *J. Vac. Sci. Technol., A* **2016**, *34*, 050605.

[20] J. Zhang, H. Yang, Q. Zhang, S. Dong, J. K. Luo, *Appl. Surf. Sci.* **2013**, *282*, 390.

[21] H. C. M. Knoops, S. E. Potts, A. A. Bol, W. M. M. Kessels, *Handbook of Crystal Growth*, Elsevier, Amsterdam, New York **2015**, pp. 1101–1134.

[22] V. Miikkulainen, M. Leskelä, M. Ritala, R. L. Puurunen, *J. Appl. Phys.* **2013**, *113*, 021301.

[23] S. E. Potts, W. Keuning, E. Langereis, G. Dingemans, M. C. M. van de Sanden, W. M. M. Kessels, *J. Electrochem. Soc.* **2010**, *157*, P66.

[24] S. C. Abrahams, J. L. Bernstein, *Acta Crystallogr. Sect. B: Struct. Crystallogr. Cryst. Chem.* **1969**, *25*, 1233.

[25] M. D. Groner, F. H. Fabreguette, J. W. Elam, S. M. George, *Chem. Mater.* **2004**, *16*, 639.

[26] S.-H. K. Park, J. Oh, C.-S. Hwang, J.-I. Lee, Y. S. Yang, H. Y. Chu, *Electrochem. Solid-State Lett.* **2005**, *8*, H21.

[27] E. Langereis, M. Creatore, S. B. S. Heil, M. C. M. Van De Sanden, W. M. M. Kessels, *Appl. Phys. Lett.* **2006**, *89*, 081915.

[28] M. Knez, A. Kadri, C. Wege, U. Gösele, H. Jeske, K. Nielsch, *Nano Lett.* **2006**, *6*, 1172.

[29] G. K. Hyde, S. D. McCullen, S. Jeon, S. M. Stewart, H. Jeon, E. G. Loboa, G. N. Parsons, *Biomed. Mater.* **2009**, *4*, 025001.

[30] A. Khan, M. Ali Abbasi, M. Hussain, Z. Hussain Ibupoto, J. Wissting, O. Nur, M. Willander, *Appl. Phys. Lett.* **2012**, *101*, 193506.

[31] A. Manekkathodi, M.-Y. Lu, C. W. Wang, L.-J. Chen, *Adv. Mater.* **2010**, *22*, 4059.

[32] Z. K. Tang, G. K. L. Wong, P. Yu, M. Kawasaki, A. Ohtomo, H. Koinuma, Y. Segawa, *Appl. Phys. Lett.* **1998**, *72*, 3270.

[33] E. B. Yousfi, J. Fouache, D. Lincot, *Appl. Surf. Sci.* **2000**, *153*, 223.

[34] J. Malm, E. Sahramo, J. Perälä, T. Sajavaara, M. Karppinen, *Thin Solid Films* **2011**, *519*, 5319.

[35] S.-Y. Pung, K.-L. Choy, X. Hou, C. Shan, *Nanotechnology* **2008**, *19*, 435609.

[36] S. Jeon, S. Bang, S. Lee, S. Kwon, W. Jeong, H. Jeon, H. J. Chang, H.-H. Park, *J. Electrochem. Soc.* **2008**, *155*, H738.

[37] N. Y. Yuan, S. Y. Wang, C. B. Tan, X. Q. Wang, G. G. Chen, J. N. Ding, *J. Cryst. Growth* **2013**, *366*, 43.

[38] A. Gibaud, G. Vignaud, *X-Ray and Neutron Reflectivity*, Springer, Berlin, Heidelberg **2009**, pp. 85–131.

[39] J. M. Jensen, A. B. Oelkers, R. Toivola, D. C. Johnson, J. W. Elam, S. M. George, *Chem. Mater.* **2002**, *14*, 2276.

[40] E. Guziewicz, M. Godlewski, L. Wachnicki, T. A. Krajewski, G. Luka, S. Gieraltowska, R. Jakiela, A. Stonert, W. Lisowski, M. Krawczyk, J. W. Sobczak, A. Jablonski, *Semicond. Sci. Technol.* **2012**, *27*, 074011.

[41] Ü. Özgür, Y. I. Alivov, C. Liu, A. Teke, M. A. Reshchikov, S. Doğan, V. Avrutin, S.-J. Cho, H. Morkoç, *J. Appl. Phys.* **2005**, *98*, 041301.

[42] Z. Liang, Q. Zhang, O. Wiranwetchayan, J. Xi, Z. Yang, K. Park, C. Li, G. Cao, *Adv. Funct. Mater.* **2012**, *22*, 2194.

[43] B. D. Viezbicke, S. Patel, B. E. Davis, D. P. Birnie, *Phys. Status Solidi* **2015**, *252*, 1700.

[44] J. F. Muth, R. M. Kolbas, A. K. Sharma, S. Oktyabrsky, J. Narayan, *J. Appl. Phys.* **1999**, *85*, 7884.

[45] N. Nandakumar, B. Dielissen, D. Garcia-Alonso, Z. Liu, R. Gortzen, W. M. M. E. Kessels, A. G. Aberle, B. Hoex, *IEEE J. Photovoltaics* **2015**, *5*, 1462.

[46] Y.-M. Chang, J. Shieh, P.-Y. Chu, H.-Y. Lee, C.-M. Lin, J.-Y. Juang, *ACS Appl. Mater. Interfaces* **2011**, *3*, 4415.

[47] D. M. Bagnall, Y. F. Chen, M. Y. Shen, Z. Zhu, T. Goto, T. Yao, *J. Cryst. Growth* **1998**, *184–185*, 605.

[48] R. C. Rai, M. Guminiak, S. Wilser, B. Cai, M. L. Nakarmi, *J. Appl. Phys.* **2012**, *111*, 073511.

[49] N. Y. Yuan, S. Y. Wang, C. B. Tan, X. Q. Wang, G. G. Chen, J. N. Ding, *J. Cryst. Growth* **2013**, *366*, 43.

[50] S. T. Tan, B. J. Chen, X. W. Sun, X. Hu, X. H. Zhang, S. J. Chua, *J. Cryst. Growth* **2005**, *281*, 571.

[51] O. Lupan, T. Pauporté, L. Chow, B. Viana, F. Pellé, L. K. Ono, B. Roldan Cuenya, H. Heinrich, *Appl. Surf. Sci.* **2010**, *256*, 1895.

[52] A. Perrotta, J. Pilz, A. Milella, A. M. Coclite, *Appl. Surf. Sci.* **2019**, *483*, 10.

[53] T. A. Krajewski, P. Terziyska, G. Luka, E. Lusakowska, R. Jakiela, E. S. Vlakhov, E. Guziewicz, *J. Alloys Compd.* **2017**, *727*, 902.

[54] T. A. Krajewski, K. Dybko, G. Luka, E. Guziewicz, P. Nowakowski, B. S. Witkowski, R. Jakiela, L. Wachnicki, A. Kaminska, A. Suchocki, M. Godlewski, *Acta Mater.* **2014**, *65*, 69.

[55] J. G. E. Gardeniers, Z. M. Rittersma, G. J. Burger, *J. Appl. Phys.* **1998**, *83*, 7844.